

Determination of the charge transport abilities of polymorphs $[C_6F_5Cu]_2(4,4'-bipy)$ with different interactions: a density functional theoretical investigation

Fei Yu · Guochun Yang · Shuixing Wu ·
Yun Geng · Zhongmin Su

Received: 29 September 2010/Accepted: 23 December 2010/Published online: 11 January 2011
© Springer-Verlag 2011

Abstract Due to the different molecular stacking conformations, two kinds of intermolecular interactions, arene–arene π -stacking interaction and Cu–Cu interaction coexist in the polymorphs of $[C_6F_5Cu]_2(4,4'-bipy)$ crystals, **3- α** and **3- β** . However, the relative magnitude of the two kinds of intermolecular interactions in **3- α** and **3- β** is different. With the help of first-principle band structure calculations, the relationship between the charge transport abilities and the intermolecular interactions in the two polymorphs was investigated for the first time. The analysis of band structures and Γ point wave functions of the band-edge state in the valence band of crystal **3- α** shows that the Cu–Cu interaction so-called cuprophilic interaction determines the hole transport ability, although this interaction is weaker than that in crystal **2** of $C_6F_5Cu(py)$ discussed in our previous work, which is a promising hole transport material. For polymorph crystal **3- β** , the wave functions of LUMO are mainly localized on the bipyridine (bpy) groups, which are result from the arene–arene π -stacking interaction between the bpy groups. Such a π – π stacking interaction dominates the electron transport ability in the conduction band of **3- β** and makes the electron main carrier for transporting. The results are also supported by the analysis of effective masses and density of states (DOS). Thus, the charge transport properties are dominated by different intermolecular interactions due to the different molecule stacking in the two polymorphs.

Keywords $[C_6F_5Cu]_2(4,4'-bipy)$ · Cuprophilic interaction · π -stacking interaction · Polymorph · Charge transport

1 Introduction

The pioneering work of efficient green electroluminescence material tris(8-hydroxyquinolate)aluminum (**Alq₃**) discovered by Tang and Slyke has stimulated the growing interests in organic materials using in organic light-emitting diodes (OLEDs) [1]. In recent years, five crystalline polymorphs (α , β , γ , δ , and ϵ) of **Alq₃** have been identified [2–6], which have the same chemical composition but the molecular configuration and packing in crystals are different. It was found that the form of the molecular packing affects not only the optical properties of **Alq₃** [2, 3, 7, 8] but also the charge transport properties [9]. It is well known that mer-**Alq₃** is an excellent electron transport material. Recently, a facile double-film annealing approach has been developed to controllably construct mer- and fac-**Alq₃** nano/microrods as well as their nano/microrod-based thin films. Current–voltage characteristics of a hole-only device implied that fac-**Alq₃** is a typical hole transport material, which is totally different from mer-**Alq₃** [9].

The variety in polymorphs offers more possibilities for new characters. With different polymorphs, their optical and electronic characteristics could be quite distinct [10–15]. Wang and co-workers designed and synthesized a series of organic polymorphic luminescent crystals constructed by 3(5)-(9-anthryl)pyrazole (**ANP**), and their optical properties are different resulting from their unique interactions based on hydrogen bonding and π – π stacking interactions. Moreover, some of them produce blue-emissive crystals with high quantum yields, suggesting their potentials as

F. Yu · G. Yang (✉) · S. Wu · Y. Geng · Z. Su (✉)
Institute of Functional Material Chemistry,
Faculty of Chemistry, Northeast Normal University,
130024 Changchun, People's Republic of China
e-mail: yanggc468@nenu.edu.cn

Z. Su
e-mail: zmsu@nenu.edu.cn

blue emitters in the optoelectronics [16, 17]. Recently, Fu et al. prepared a series of polymorphs using rubrene molecules, ranging from 1D ribbons to 2D rhombic and hexagonal plates exhibiting totally different optical properties [18]. It is probably related to their different solid-state structures, which might exploit the potential of organic small molecules in optic and opto-electronic devices.

Especially for organic small-molecular semiconductors, charge transport is closely related to the crystal-packing motif, and different packing modes in crystals strongly influence the carrier mobility [19–22]. Troisi et al. [23] calculated the band structures of the four polymorphs of pentacene and found that the mobility is extremely anisotropic for polymorphs I–III, which is highly relevant to the application of pentacene thin layers in an organic transistor. Replacing two carbon atoms with nitrogen atoms of pentacene, three polymorphs of 6,13-dihydro-6,13-diaza-pentacene (**DHDAP**) crystals were obtained, and the field effect mobility is extremely sensitive to the polymorph with the “12.9 Å phase” yielding a mobility of $0.45 \text{ cm}^2 \text{ V}^{-1} \text{ s}^{-1}$, which is over 5,000 times higher than those of the other phases [24].

A deep understanding of the charge transport mechanism resulting from different weak interactions in polymorphs is fundamental and important for the design and application in organic optoelectronic devices. In our previous work, we found that the crystal **2** of $\text{C}_6\text{F}_5\text{Cu}(\text{py})$ is a promising hole transport material with the cuprophilic interactions [25]. With the 2:1 treatment of $\text{C}_6\text{F}_5\text{Cu}$ and 4,4'-bipyridine, two polymorphs, $[\text{C}_6\text{F}_5\text{Cu}]_2(\text{bpy})$, namely, crystal **3- α** and **3- β** are obtained. Unlike crystal **2** with the ligands in a staggered conformation, both the polymorphs **3- α** and **3- β** show supramolecular two-dimensional stacks as a result of multiple perfluoroarene–arene π -interactions. Besides, the cuprophilic interactions may also exist in the two polymorphs and influence the charge transport properties [26]. To the best of our knowledge, no theoretical study on the charge transport properties of polymorphs involving multiple intermolecular interactions has been reported in the literature. Thus, it is an ideal model to investigate the internal mechanism influencing the transport abilities with different interactions in the polymorphs.

2 Theoretical methodology

Generally, there are two models to describe the charge transport mechanism at present: hopping model and band-like model. The charge transport is governed by hopping mechanism when the system is disordered at room temperature. But in the well-ordered organic crystals, the mobility is more rationally described by band-like model.

In a standard band-theory model, the group velocity $v(k)$ of the delocalized electron waves or hole waves is given by the gradient of the band energy in k -space,

$$\vec{v}(k) = \nabla_k E(k) / \hbar \quad (1)$$

where $E(k)$ is the band structure of the system, k the wave vector, and $\hbar = h/2\pi$, h is the Planck constant. Under the constant relaxation time approximation at low temperature, the mobility can be given by

$$\mu_\alpha = e t m_\alpha^{-1} \quad (2)$$

Here, the inverse effective mass m_α^{-1} is a key parameter of the charge transport in the band-like model. The effective mass is related to the curvature of the minimum/maximum of the conductive band (CB)/valence band (VB). It reads

$$m_{\alpha\beta}^{-1} = -\frac{1}{\hbar^2} \left(\frac{\partial^2 E(k)}{\partial k_\alpha \partial k_\beta} \right) \quad (3)$$

Here, subscripts α and β denote the Cartesian coordinates in reciprocal space, and $E(k)$ is the band energy. The heavier the effective mass is, the smaller the mobility is. The interaction (or binding) energy in a dimer extracted from a crystallographic structure is calculated as

$$\Delta E = E_{\text{dimer}} - 2E_{\text{monomer}} \quad (4)$$

Here, E_{dimer} is the total energy of the dimer in the fixed crystallographic structure, and E_{monomer} is the energy of an isolated monomer. Generally, the larger binding energy is, the stronger intermolecular interaction is.

Density functional theory (DFT) [27, 28] calculations are carried out using Dmol³ within the Material Studio package [29, 30]. It should be noted that there are certain limitations of current DFT functionals in accurately describing van der Waals forces in the molecular crystals. Byrd et al. [31] have systematically tested the successes and failures of current DFT functionals and suggested that it is necessary to develop new DFT functionals which include accurate dispersion forces. In this paper, the generalized gradient approximation (GGA) in Perdew–Burke–Ernzerhof (PBE) [32] form and all-electron double numerical basis set with polarized function (DNP basis set) are used to calculate the band structures and Γ point wave functions. The lattice parameters used here for **3- α** are $a = 8.071 \text{ \AA}$, $b = 11.127 \text{ \AA}$, $c = 48.264 \text{ \AA}$, and $\alpha = \beta = \gamma = 90^\circ$ and for **3- β** , $a = 9.288 \text{ \AA}$, $b = 5.033 \text{ \AA}$, $c = 22.316 \text{ \AA}$, and $\alpha = \gamma = 90^\circ$, $\beta = 92.57^\circ$ [26]. Integrations over the Brillouin zone were sampled by $6 \times 4 \times 1$ k points for **3- α** and $4 \times 8 \times 2$ k points for **3- β** , using the Monkhorst–Pack scheme [33]. The binding energy between the monomers in polymorphs **3- α** is calculated under MP2 [34] level as implemented in the Gaussian 09 program [35]. Basis sets of SDD [36, 37] containing relativistic effects were applied to

metal atoms and 6-31G** [38, 39] were applied to C, H, N, and F. The basis set superposition errors (BSSE) [40] were taken into consideration in binding energy calculations.

3 Results and discussion

3.1 Crystal structures

Jäkle and co-workers designed and synthesized the two polymorphs of $[C_6F_5Cu]_2(4,4'\text{-bipy})$ with slow diffusion of a solution of 4,4'-bipyridine in CH_2Cl_2 into a solution of $[C_6F_5Cu]_4$, which are described in detail in Ref [26]. Figure 1 displays a graphical representation of the molecular structure and packing mode of the two polymorphs, **3- α** and **3- β** . They have the same chemical composition $[C_6F_5Cu]_2(4,4'\text{-bipy})$, and the copper centers in their structures adopt a linear or nearly linear coordination geometry (**3- α** : 180° ; **3- β** : 178.17°). The pentafluorophenyl groups and the pyridine rings are nearly coplanar, with an angle of 3.8° for **3- α** and 9.5° for **3- β** . The main difference of the two structures is in the twist at the central C–C bond connecting the two pyridines: there is an interplanar angle of 44.3° in **3- α** , but it is a coplanar conformation adopted in the pyridines in **3- β** . Thus, the whole molecule in **3- β** exhibits a much more planar conformation than that in **3- α** (see the monomer molecular structures in Fig. 1). From the viewpoint of crystal packing, differing from the staggered

conformation of the ligands in adjacent units in crystal **2**, the polymorphs of **3- α** and **3- β** exhibit a supramolecular two-dimensional stacks as a result of multiple perfluoroarene–arene interactions. The molecules in **3- α** arrange along the long axis of *c*, and the pentafluorophenyl groups are adopted a coplanar conformation with the pyridines rings of adjacent molecules. The interplanar distance between the aromatic rings is around 3.5 \AA , which is a typical distance of arene–arene π -packing interactions, while the copper atoms are arranged in a zigzag conformation and the distance between copper atoms is about 3.639 \AA , which is much longer than that in crystal **2** (2.893 \AA). In the polymorph of **3- β** , the molecules arrange along the *b*-axis with a much larger offset compared with **3- α** , thus resulting in the alignment of copper atoms is 5.033 \AA in distance, which is much longer than that in **3- α** . But the distance between the bipyridine groups in adjacent molecules is only 3.461 \AA , which is smaller than the Cu–Cu distance and also the distance between aromatic rings in **3- α** .

3.2 Band structures

The crystal of **3- α** crystallizes in the orthorhombic space group *FDDD*, while **3- β** crystallizes in the monoclinic space group *P21/n*. We calculated the band structures of **3- α** and **3- β** using Dmol³ in Materials Studio package along high-symmetry directions. The high-symmetry coordinates for **3- α** are $R(1/2, 1/2, 0)$, $\Gamma(0, 0, 0)$, $X(1/2, 0, 0)$, $Y(0, 1/2, 0)$,

Fig. 1 Crystal structures of **3- α** , **3- β** , and their monomer molecular structures

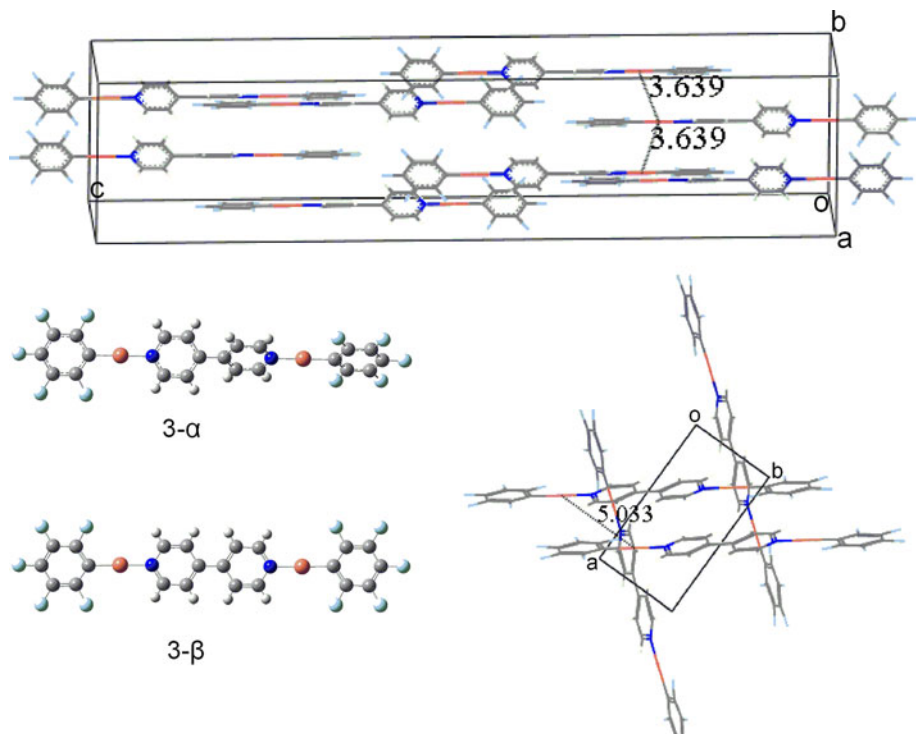


Fig. 2 Band structures of **3- α** (left) and **3- β** (right)

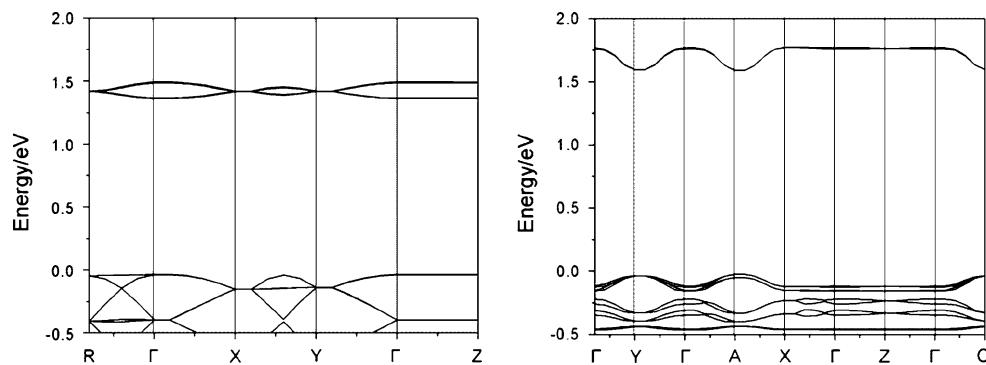


Table 1 Bandwidths in VB and CB of **3- α** and **3- β** along high-symmetry directions in eV

3-α	VB	CB
$\text{R}\Gamma$	0.01	0.05
ΓX	0.12	0.05
XY	0.11	0.03
$\text{Y}\Gamma$	0.10	0.05
ΓZ	0	0
3-β	VB	CB
ΓY	0.08	0.16
ΓA	0.09	0.17
AX	0.10	0.18
$\text{X}\Gamma$	0.01	0.01
ΓZ	0	0.01
ΓC	0.08	0.16

and $\text{Z}(0, 0, 1/2)$ and for **3- β** , $\Gamma(0, 0, 0)$, $\text{Y}(0, 1/2, 0)$, $\text{A}(1/2, 1/2, 0)$, $\text{X}(1/2, 0, 0)$, $\text{Z}(0, 0, 1/2)$, and $\text{C}(0, 1/2, 1/2)$. The calculated band structures are shown in Fig. 2. They are both direct semiconductors with its maximum of valence band and minimum of conduction band at Γ point in crystal **3- α** and at A point in crystal **3- β** , respectively.

It is clear that the unoccupied bands are degenerate but the occupied bands are not in **3- α** . The larger bandwidths are along high-symmetry lines $\Gamma \rightarrow \text{X}$, $\text{X} \rightarrow \text{Y}$, and $\text{Y} \rightarrow \Gamma$ compared with other high-symmetry directions. Moreover, the bandwidths in valence band (VB) are much larger than those in conduction band (CB), which are listed in Table 1. These high-symmetry lines are corresponding to the directions where arene–arene π -packing interaction takes place and also the directions of copper atoms arranging in a zigzag conformation.

In the band structure of crystal **3- β** , both occupied bands and unoccupied bands consist of two subbands. The larger bandwidths of both valence band and conduction band are along high-symmetry lines $\Gamma \rightarrow \text{Y}$, $\Gamma \rightarrow \text{A}$, $\text{A} \rightarrow \text{X}$, and $\Gamma \rightarrow \text{C}$ compared with other high-symmetry directions. Furthermore, the bandwidths in conduction band are larger

Table 2 Hole and electron effective masses m (in units of the electron mass at rest, m_0) along different directions of the **3- α** and **3- β** crystals

	Hole (m/m_0)	Electron (m/m_0)
3-α		
ΓX	2.22	4.97
XY	1.19	4.72
$\text{Y}\Gamma$	1.34	2.51
3-β		
ΓY	7.37	3.72
ΓA	3.01	1.62
AX	6.18	3.35

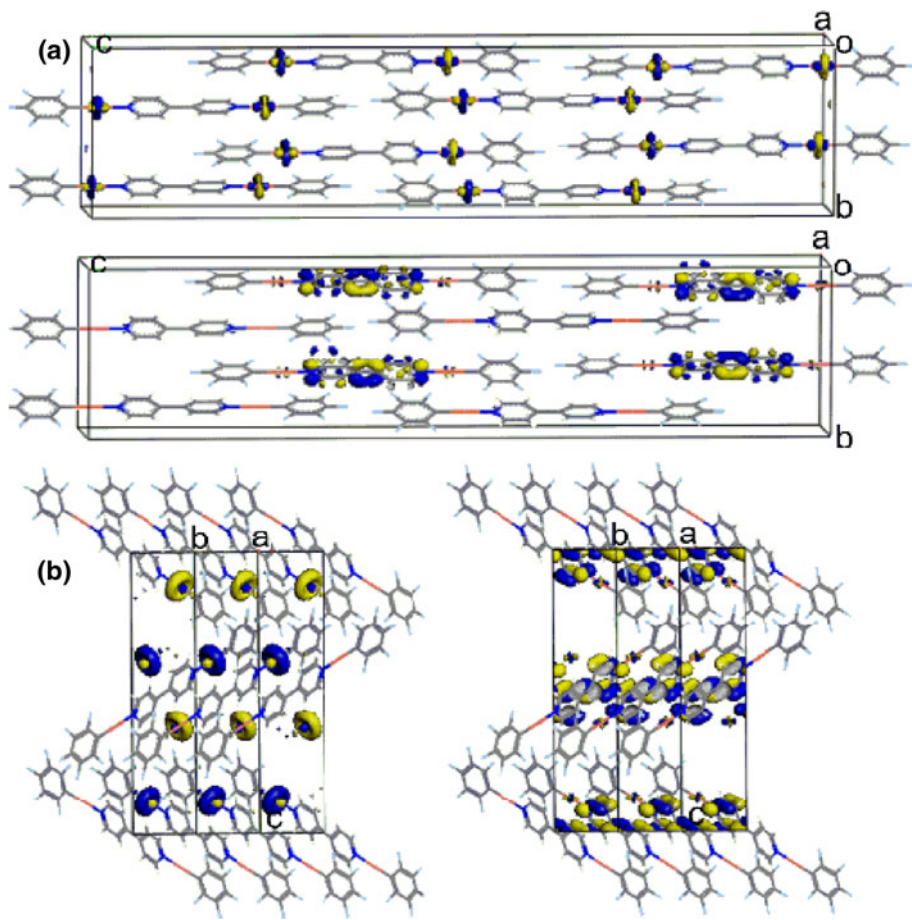
than that in valence band, which is different with that in **3- α** . Among the larger dispersive directions, $\Gamma \rightarrow \text{Y}$ corresponds to the b -axis direction in real space, which is the direction of arene–arene π – π interaction, and copper atoms arranged in a distance 5.033 Å alignment, is also along this direction.

We also calculated the hole and electron effective masses at the band extrema along high-symmetry lines in crystal **3- α** and **3- β** , which are listed in Table 2. From the viewpoint of band model, the smaller effective mass is, the larger mobility is. The hole effective masses are all smaller than electron ones in **3- α** , indicating that hole is the main carrier for transporting. While in crystal **3- β** , the electron effective masses are all smaller than hole ones, which means that electron is main carrier for transporting. These results are consistent with the analysis of band structures.

3.3 Frontier molecular orbitals

There is a close relationship between the charge transport and distribution of frontier molecular orbitals. The wave functions of the band-edge state at the Γ point of crystals **3- α** and **3- β** are shown in Fig. 3, which are equivalent to the frontier molecular orbitals, namely, the HOMO for hole and LUMO for electron. Here, the yellow (blue) color is for

Fig. 3 Γ point wave functions of **a** $3\text{-}\alpha$ (top HOMO, bottom LUMO) and **b** $3\text{-}\beta$ (left HOMO, right LUMO)

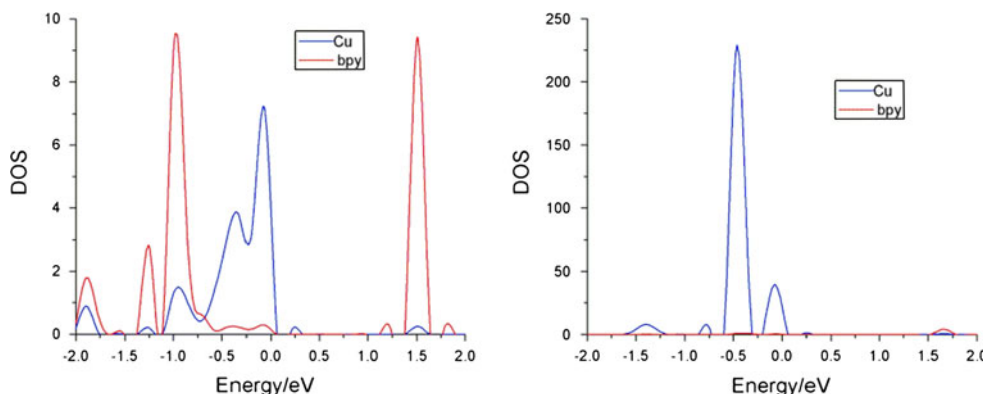


positive (negative) wave functions values. Sometimes, the extreme point of valence band or conduction band is not at Γ point. For example, Shuai et al. calculated the band structure of Alq_3 and analyzed the Γ point wave functions from the viewpoint of band model. In their case, the extreme point of valence band is at X point, not at the Γ point, but it also gives reliable results [41]. As seen from the illustration of $3\text{-}\alpha$, the wave functions of HOMO display a significant electronic density on the copper atoms. The copper atoms are aligned with Cu–Cu distance of 3.639 Å, and the cuprophilic interaction might still exist in such a Cu–Cu distance. We calculated the binding energy between monomers. The binding energy is -6.07 kcal/mol, which is smaller than -7.12 kcal/mol in crystal **2** in our previous work because of a longer Cu–Cu distance of 3.639 Å. Although the Cu–Cu distance is longer than that in crystal **2** (2.982 Å), the cuprophilic interaction between the copper atoms still exists and dominates the charge transport ability of holes in the valence band in crystal $3\text{-}\alpha$. While for LUMO, the wave functions are mainly on the biphenyl (bpy) groups, but there is no occupation on the pentafluorophenyl groups that adopted a coplanar conformation with the bpy. Thus, the orbital overlap between the pentafluorophenyl and bpy is small in the LUMO, which

leads to a smaller bandwidth in conduction band compared with that in valence band listed in Table 1. So, the hole is the main transport carrier, and the cuprophilic interaction determines the hole transport in $3\text{-}\alpha$.

From the illustration of $3\text{-}\beta$, we can see that the wave functions of HOMO have the same situation as that in $3\text{-}\alpha$, displaying a significant electronic density on the copper atoms. But the distance of 5.033 Å between copper atoms is too large and the cuprophilic interaction might not play a key role in determining the carrier transport ability in $3\text{-}\beta$, which can also be reflected from the band structure that the dispersion in valence band is smaller compared with that in conduction band. On the other hand, the LUMO localizes mainly on all of the biphenyl (bpy) groups, and the interplanar distance of biphenyl rings between the adjacent molecules is only 3.461 Å, which is much smaller than the Cu–Cu distance and also smaller than the distance in $3\text{-}\alpha$ of 3.50 Å between the aromatic rings. The orbital overlap between the aromatic rings in $3\text{-}\beta$ is larger than that of $3\text{-}\alpha$, so the arene–arene interaction determines the charge transport ability for electron in conduction band, which makes a larger dispersion in conduction band than that in valence band. Thus, crystal $3\text{-}\beta$ could act as the electron transport material.

Fig. 4 Density of states (DOS) of **3- α** (left) and **3- β** (right)



3.4 Density of states

To further test the conclusion drawn from frontier molecular orbitals, density of states (DOS) of the two crystals were also calculated, which is shown in Fig. 4. In **3- α** , copper atoms mainly contribute to the valence band and bipyridine (bpy) groups to the conduction band. However, the DOS of copper atom is much smaller than that of bipyridine (bpy) groups. In the case of **3- β** , copper atoms mainly contribute to valence band, but bpy groups slightly contribute to conduction band. This is also reflected from the frontier molecular orbitals. From the viewpoint of band model, the smaller DOS is, the larger bandwidth is. From the illustrations of DOS, copper atoms dominate the hole transport in **3- α** , and bpy groups dominate the electron transport in **3- β** , which is consistent with the analysis of band structures.

4 Conclusions

With the help of first-principle band structure calculations, we calculated the band structures of polymorphs of crystal **3- α** and **3- β** and analyzed the Γ point wave functions of the band-edge state. We found that different interactions dominate the charge transport abilities resulting from the unique molecule packing in the two polymorphs. From the viewpoint of band structure, the dispersion in valence band is larger than that in conduction band in **3- α** , while it is reverse in the polymorph **3- β** . On the other hand, the wave functions of LUMO in **3- α** display a significant electronic density on the bpy groups, but there is no occupation on the pentafluorophenyl groups that adopted a coplanar conformation with the bpy. So, the orbital overlap between the perfluoroarene–arene π -interaction is small. On the contrary, the HOMO are mainly localized on the copper atoms, and the cuprophilic interaction exists and dominates the charge transport ability of holes in **3- α** and hole is the main transporting carrier. In the case of **3- β** , all of the bipyridine

(bpy) groups have a main contribution on the wave functions of LUMO, and the overlap between the π -stacking bpy groups is large. However, the distances between copper atoms are too large to determine the hole transport ability. Thus, the arene–arene π -stacking interaction is the dominant factor in determining the electron transport ability in the conduction band, and electron is the main carrier for transporting in **3- β** . Understanding the different mechanisms in determining the charge transport abilities resulting from the unique molecular arrangement in polymorphs may help us design and exploit the potential organic small molecules in organic electronic devices.

Acknowledgments The authors gratefully acknowledge the financial support from the National Natural Science Foundation of China (Project No. 20703008; 20903020), National Basic Research Program of China (973 Program—2009CB623605), the Science and Technology Development Project Foundation of Jilin Province (20090146), the Training Fund of NENU’s Scientific Innovation Project (NENU-STC08005 and -STC08012), The Project-sponsored by SRF for ROCS, SEM.

References

- Tang CW, VanSlyke SA (1987) Appl Phys Lett 51:913. doi: [10.1063/1.98799](https://doi.org/10.1063/1.98799)
- Brinkmann M, Gadret G, Muccini M, Taliani C, Masciocchi N, Sironi A (2000) J Am Chem Soc 122:5147. doi: [10.1021/ja993608k](https://doi.org/10.1021/ja993608k)
- Colle M, Dinnebier RE, Brüttung W (2002) Chem Comm 2908. doi: [10.1039/b209164j](https://doi.org/10.1039/b209164j)
- Rajeswaran M, Blanton TN (2005) J Chem Cryst 35:71. doi: [10.1007/s10870-005-1157-4](https://doi.org/10.1007/s10870-005-1157-4)
- Colle M, Brüttung W (2004) Phys Stat Sol A 201:1095. doi: [10.1002/pssa.200404341](https://doi.org/10.1002/pssa.200404341)
- Colle M, Gmeiner J, Milius W, Hillebrecht H, Brüttung W (2003) Adv Funct Mater 13:108. doi: [10.1002/adfm.200390015](https://doi.org/10.1002/adfm.200390015)
- Muccini M, Brinkmann M, Gadret G, Taliani C, Masciocchi N, Sironi A (2001) Synth Met 122:31. doi: [10.1016/s0379-6779\(00\)01330-8](https://doi.org/10.1016/s0379-6779(00)01330-8)
- Braun M, Gmeiner J, Tzolov M, Coelle M, Meyer FD, Milius W, Hillebrecht H, Wendland O, von Schutz JU, Brüttung W (2001) J Chem Phys 114:9625. doi: [10.1063/1.1369157](https://doi.org/10.1063/1.1369157)
- Bi H, Zhang H, Zhang Y, Gao H, Su Z, Wang Y (2010) Adv Mater 22:1631. doi: [10.1002/adma.200903094](https://doi.org/10.1002/adma.200903094)

10. Naumov P, Kowalik J, Solntsev KM, Baldridge A, Moon J-S, Kranz C, Tolbert LM (2010) *J Am Chem Soc* 132:5845. doi: [10.1021/ja100844m](https://doi.org/10.1021/ja100844m)
11. Zhao Y, Gao H, Fan Y, Zhou T, Su Z, Liu Y, Wang Y (2009) *Adv Mater* 21:3165. doi: [10.1002/adma.200803432](https://doi.org/10.1002/adma.200803432)
12. Fan Y, Song W, Yu D, Ye K, Zhang J, Wang Y (2009) *Cryst EngComm* 11:1716
13. Mutai T, Tomoda H, Ohkawa T, Yabe Y, Araki K (2008) *Angew Chem Int Ed* 47:9522. doi: [10.1002/anie.200803975](https://doi.org/10.1002/anie.200803975)
14. Zhang H, Zhang Z, Zhang J, Ye K, Gao H, Wang Y (2007) *CrystEngComm* 9:951
15. Mutai T, Satou H, Araki K (2005) *Nat Mater* 4:685. doi: [10.1038/nmat1454](https://doi.org/10.1038/nmat1454)
16. Zhang H, Zhang Z, Ye K, Zhang J, Wang Y (2006) *Adv Mater* 18:2369. doi: [10.1002/adma.200600704](https://doi.org/10.1002/adma.200600704)
17. Zhang Z, Zhang Y, Yao D, Bi H, Javed I, Fan Y, Zhang H, Wang Y (2009) *Cryst Growth Des* 9:5069. doi: [10.1021/cg9008569](https://doi.org/10.1021/cg9008569)
18. Huang L, Liao Q, Shi Q, Fu H, Ma J, Yao J (2010) *J Mater Chem* 20:159
19. Sancho-Garcia JC, Perez-Jimenez AJ, Olivier Y, Cornil J (2010) *Phys Chem Chem Phys* 12:9381
20. Salman S, Delgado MCR, Coropceanu V, Brédas J-L (2009) *Chem Mater* 21:3593. doi: [10.1021/cm901128j](https://doi.org/10.1021/cm901128j)
21. Mas-Torrent M, Hadley P, Bromley ST, Ribas X, Tarrés J, Mas M, Molins E, Veciana J, Rovira C (2004) *J Am Chem Soc* 126:8546. doi: [10.1021/ja048342i](https://doi.org/10.1021/ja048342i)
22. Widany J, Daminelli G, Di Carlo A, Lugli P, Jungnickel G, Elstner M, Frauenheim T (2001) *Phys Rev B* 63:233204
23. Troisi A, Orlandi G (2005) *J Phys Chem B* 109:1849. doi: [10.1021/jp0457489](https://doi.org/10.1021/jp0457489)
24. Tang Q, Zhang D, Wang S, Ke N, Xu J, Yu JC, Miao Q (2009) *Chem Mater* 21:1400. doi: [10.1021/cm9001916](https://doi.org/10.1021/cm9001916)
25. Yu F, Wu SX, Geng Y, Yang GC, Su ZM (2010) *Theo Chem Acc.* doi: [10.1007/s00214-010-0785-8](https://doi.org/10.1007/s00214-010-0785-8)
26. Sundararaman A, Zakharov LN, Rheingold AL, Jäkle F (2005) *Chem Comm* 1708. doi: [10.1039/b417532h](https://doi.org/10.1039/b417532h)
27. Yang CH, Su WL, Fang KH, Wang SP, Sun IW (2006) *Organometallics* 25:4514. doi: [10.1021/om060323p](https://doi.org/10.1021/om060323p)
28. Liu T, Zhang HX, Xia BH (2007) *J Phys Chem A* 111:8724. doi: [10.1021/jp072802n](https://doi.org/10.1021/jp072802n)
29. Dellec B (1990) *J Chem Phys* 92:508. doi: [10.1063/1.458452](https://doi.org/10.1063/1.458452)
30. Dellec B (2000) *J Chem Phys* 113:7756. doi: [10.1063/1.1316015](https://doi.org/10.1063/1.1316015)
31. Byrd EFC, Scuseria GE, Chabalowski CF (2004) *J Phys Chem B* 108:13100. doi: [10.1021/jp0486797](https://doi.org/10.1021/jp0486797)
32. Perdew JP, Burke K, Ernzerhof M (1996) *Phys Rev Lett* 77:3865. doi: [10.1103/PhysRevLett.77.3865](https://doi.org/10.1103/PhysRevLett.77.3865)
33. Pack JD, Monkhorst HJ (1977) *Phys Rev B* 16:1748
34. Head Gordon M, Pople JA, Frisch MJ (1988) *Chem Phys Lett* 153:503. doi: [10.1016/0009-2614\(88\)85250-3](https://doi.org/10.1016/0009-2614(88)85250-3)
35. Frisch MJ, Trucks GW, Schlegel HB, Scuseria GE, Robb MA, Cheeseman JR, Scalmani G, Barone V, Mennucci B, Petersson GA, Nakatsuji H, Caricato M, Li X, Hratchian HP, Izmaylov AF, Bloino J, Zheng G, Sonnenberg JL, Hada M, Ehara M, Toyota K, Fukuda R, Hasegawa J, Ishida M, Nakajima T, Honda Y, Kitao O, Nakai H, Vreven T, Montgomery JA Jr, Peralta JE, Ogliaro F, Bearpark M, Heyd JJ, Brothers E, Kudin KN, Staroverov VN, Kobayashi R, Normand J, Raghavachari K, Rendell A, Burant JC, Iyengar SS, Tomasi J, Cossi M, Rega N, Millam JM, Klene M, Knox JE, Cross JB, Bakken V, Adamo C, Jaramillo J, Gomperts R, Stratmann RE, Yazyev O, Austin AJ, Cammi R, Pomelli C, Ochterski JW, Martin RL, Morokuma K, Zakrzewski VG, Voth GA, Salvador P, Dannenberg JJ, Dapprich S, Daniels AD, Farkas O, Foresman JB, Ortiz JV, Cioslowski J, Fox DJ (2009) Gaussian 09, Revision A.02, Gaussian, Inc., Wallingford CT
36. Özen C, Tütün NS (2008) *Organometallics* 27:4600. doi: [10.1021/om800094k](https://doi.org/10.1021/om800094k)
37. Geisberger G, Klapötke TM, Stierstorfer J (2007) *Eur J Inorg Chem* 2007:4743. doi: [10.1002/ejic.200700395](https://doi.org/10.1002/ejic.200700395)
38. Ditchfield R, Hehre WJ, Pople JA (1971) *J Chem Phys* 54:724. doi: [10.1063/1.1674902](https://doi.org/10.1063/1.1674902)
39. Gordon MS (1980) *Chem Phys Lett* 76:163. doi: [10.1016/0009-2614\(80\)80628-2](https://doi.org/10.1016/0009-2614(80)80628-2)
40. Boys SF, Bernardi F (1970) *Mol Phys* 19:553. doi: [10.1080/00268977000101561](https://doi.org/10.1080/00268977000101561)
41. Yang YT, Geng H, Yin SW, Shuai ZG, Peng JB (2006) *J Phys Chem B* 110:3180. doi: [10.1021/jp0540252](https://doi.org/10.1021/jp0540252)